Available online at www.sciencedirect.com

SCIENCE DIRECT®

Tectonophysics 407 (2005) 117–134

TECTONOPHYSICS

www.elsevier.com/locate/tecto

Intrusion and its implication for subsidence: A case from the Baiyun Sag, on the northern margin of the South China Sea

Xiaobin Shi [a,*], Evgenii Burov [b], Sylvie Leroy [b], Xuelin Qiu [a], Bin Xia [c]

[a] *Key Laboratory of the Marginal Sea Geology, South China Sea Institute of Oceanology, Chinese Academy of Sciences, 164, Xingang Xi Road, Guangzhou, 510301, China*

[b] *Laboratoire de Tectonique UMR 7072, Universite de Pierre et Marie Curie, Paris, France*

[c] *Key Laboratory of the Marginal Sea Geology, Guangzhou Institute of Geochemistry, Chinese Academy of Sciences, P.O. Box 1131, Guangzhou, 510640, China*

Received 11 March 2004; accepted 20 July 2005
Available online 26 August 2005

Abstract

We develop a series of simple numerical models to explain the anomalous subsidence and deposition phenomena on the northern continental margin of the South China Sea, in particular in the Baiyun Sag. The results suggest that a short-period high rate deposition of around 17 Ma is related to a rapid subsidence event, which may be due to episodic emplacement of a dense intrusion. Necking and gravity models indicate that in the basement of the Baiyun Sag, there is a dense zone that is 100–200 kg/m^3 more dense than the surrounding country rock. Considering its high magnetic intensity and regional igneous activity, the dense zone is thought to be related to a phase of basalt intrusion that may have taken place around 17 Ma. Thermal and subsidence models indicate that a hot denser intrusion can cause significant subsidence immediately after the intrusion. The subsidence rate then slows down with cooling, thus becoming consistent with the observed subsidence curves at around 17 Ma. The results also indicate that the lithospheric strength under the Baiyun Sag is negligible, and that the high-velocity layer in the lowermost crust may be not an original part of the pre-rift crust. Instead, it is thought to be underplated intrusion emplaced at around 30 Ma when the continental margin broke up.

Keywords: Intrusion; Subsidence; High velocity layer; South China Sea

1. Introduction

Passive continental margins are associated with continental rifting and the subsequent formation of ocean basins. These margins often experience large subsidence and develop oil and gas bearing sedimentary basins filled with important amounts of sediments. For example, the largest sediment thickness is more than 10 km offshore eastern northern America (Chian et al., 1995) and South China (Pang et al., 2004). It is commonly accepted that the main factors

* Corresponding author. Fax: +86 20 8445 1672.
E-mail address: xbshi@scsio.ac.cn (X. Shi).

0040-1951/$ - see front matter © 2005 Elsevier B.V. All rights reserved.
doi:10.1016/j.tecto.2005.07.004

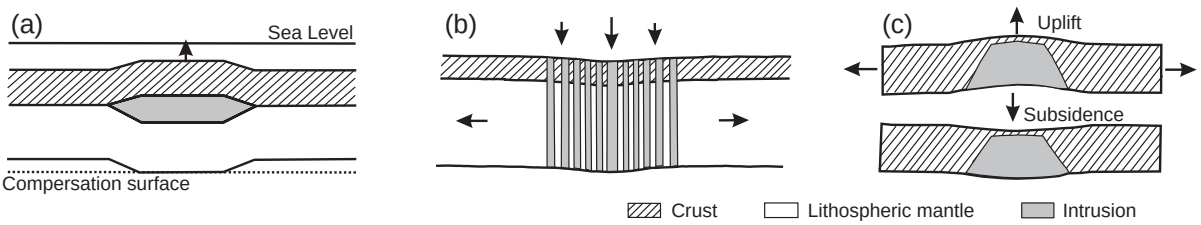

Fig. 1. (a) Underplated intrusion causing surface uplift (Watts, 2001). (b) Extension model of dike intrusion into lithosphere (Royden et al., 1980). (c) Dense intrusion into crust, causing extension, and/(or no) surface uplift and erosion (upper), followed by quick subsidence (bottom).

responsible for the subsidence of rifted basins are crustal thinning, lithospheric cooling and sedimentary loading (Watts and Torne, 1992). Though these three factors play together a key role in the subsidence of passive continental margins, other factors, such as inelastic yielding caused by loading (Burov and Diament, 1995), and emplacement of dense bodies (magmatic or phase changes), may also play an additional role.

In addition to sedimentary loading, magmatic bodies that have been intruded into the crust during the rifting and post-rifting phases may enhance or weaken subsidence, depending on the density of material they replace, and should be taken into account. Watts (2001) argued that an underplated body below crust would result in buoyancy-driven uplift because of its lower density than mantle material (Fig. 1a). Royden et al. (1980) suggested a model that considers cracking of the continental lithosphere and intrusion of dikes or diapirs from the mantle (Fig. 1b). Replacement of light crustal rocks by denser ultrabasic or basaltic material results in initial rapid subsidence and later long-term thermal subsidence. The high-temperature dense crustal intrusion may also cause uplift with or without coeval erosion depending on the water depth. This uplift is rapidly relayed by subsidence caused by denser intrusion and by the removal of crustal material (Fig. 1c). This mechanism (Fig. 1c) was employed by Ludmann and Wong (1999) and Ludmann et al. (2001) to explain the two magmato-tectonic uplift events and subsequent subsidence centered on the Dongsha Rise (Fig. 2) at Miocene/Pliocene boundary and within the lower Middle Pleistocene.

Subsidence due to a normal load depends not only on its load size and wavelength, but also on the strength (T_e) of the underlying lithosphere (Watts, 2001; Burov and Diament, 1995). T_e estimates for continental rifted margins are still a subject of active debates, although it is generally accepted that rifted margins have low strength. Recent studies confirm that the rifted crust can be weak (i.e., effective elastic thickness (T_e) <10–11 km) (Watts, 2001; Cloetingh et al., 1995; Watts and Stewart, 1998). However, it has also been shown that some rifted margins are characterized by high T_e values (Watts, 2001). The west Greenland Margins are associated with T_e values larger than 20 km, and the Atlantic Margin offshore of Nova Scotia is associated with values of 20–60 km (Keen and Dehler, 1997). One obvious geological evidence that the rifts preserve some strength is the presence of rift flanks that can remain flexurally uplifted for more than 50 my after the rift phase (Weissel and Karner, 1989; Braun and Beaumont, 1989; Chery et al., 1992). Wide rifted margins are often characterized by several depressions alternating with uplifted zones. Thus, if the lithosphere preserved its strength during the rift and post rift phases, then the subsidence of one tectonic unit may be influenced by subsidence/uplift of the neighboring unit and even by that of more distant units. Comparing results of 1D Airy backstripping and 2D flexural backstripping, Roberts et al. (1998) found that Airy models yields overestimated values for stretching factor β.

Fig. 2. (a) Location of the northern margin of the South China Sea. (b) Drills and seismic lines around the Baiyun Sag. (c) Seismic section Profile 1554 crossing the Northern Margin of the South China Sea (Wang et al., 1997). DS=Dongsha Rise, PY=Panyu Low Rise, SH=Shenhu Rise, CS=Chaoshan Depression, BYS=Baiyun Sag, ZHU III=Zhu III Depression, ZHU I=Zhu I Depression, ZHU II=ZHU II Depression, TXB=Taixi Basin, TXNB=Taixinan Basin, PH=Penghu Rise. The triangles near Profile OBS93 are the locations of the probe heat flow data (Nissen et al., 1995a).

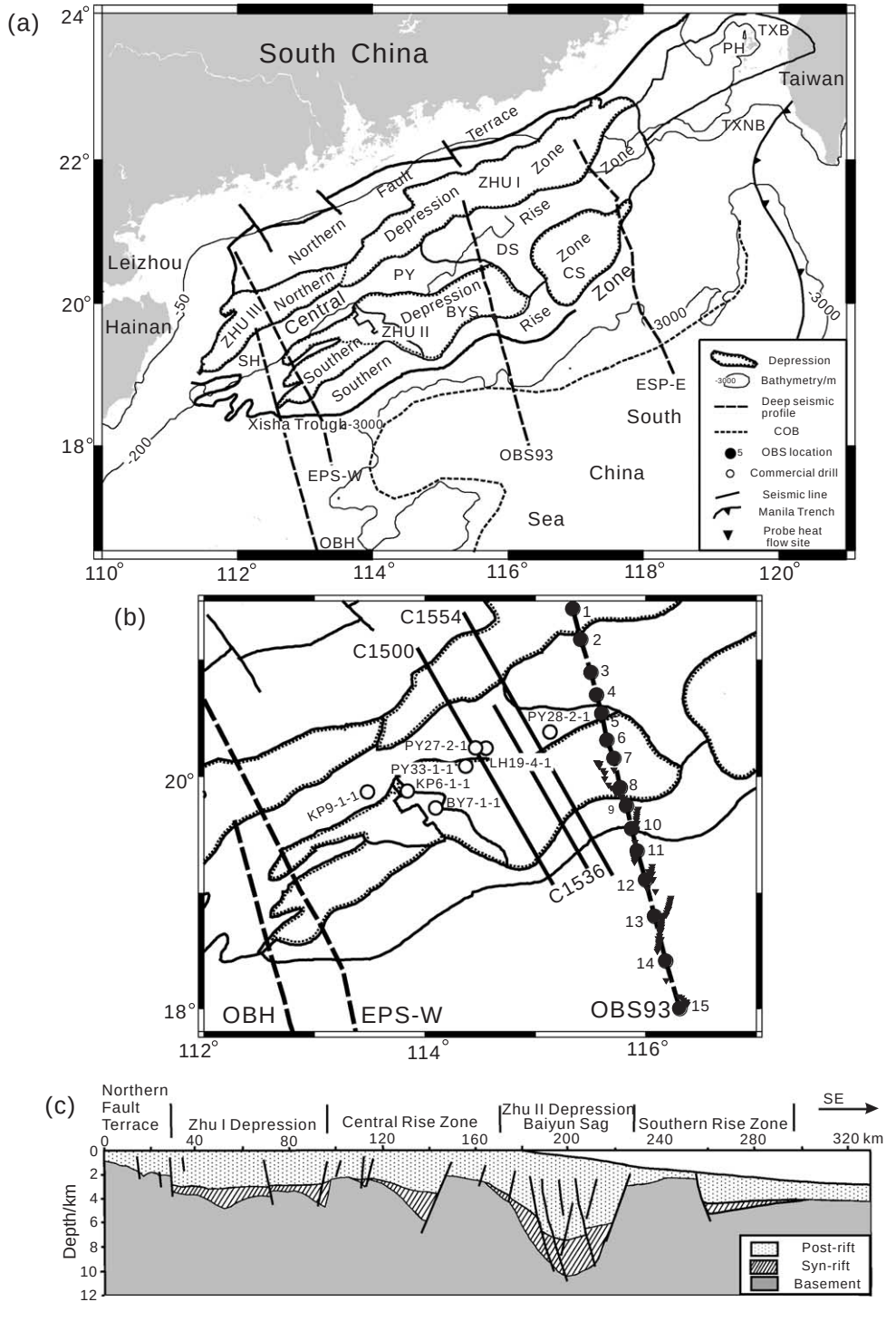
(a)
South China
Taiwan
TXB
PH
TXNB
Terrace
Fault
Zone
ZHU I
Depression
Rise
Northern
Central
Southern
ZHU II
ZHU III
DS
PY
BYS
CS
SH
Leizhou
Hainan
Xisha Trough
ESP-E
OBS93
EPS-W
OBH
South China Sea
Depression
Bathymetry/m
Deep seismic profile
COB
OBS location
Commercial drill
Seismic line
Manila Trench
Probe heat flow site
(b)
C1554
C1500
C1536
PY28-2-1
PY27-2-1
PY33-1-1
LH19-4-1
KP6-1-1
KP9-1-1
BY7-1-1
OBH
EPS-W
OBS93
(c)
Northern Fault Terrace
Zhu I Depression
Central Rise Zone
Zhu II Depression
Baiyun Sag
Southern Rise Zone
SE
320 km
Depth/km
Post-rift
Syn-rift
Basement

The South China Sea is one of the greatest marginal seas of the west Pacific (Fig. 2). Its northern continental margin is dominated by extensional structures, among which the Pearl River Mouth Basin is the largest. The results of deep seismic sounding (Nissen et al., 1995a; Yao et al., 1994, 2001) reveal a high velocity layer in the lowermost crust (Fig. 3). The nature of the high velocity layer is not clear. Though Nissen et al. (1995b) suggested that the high velocity layer presents a part of the pre-rift crust, Yan et al. (2001) argued that it is an underplated intrusion, which was emplaced after the cessation of seafloor spreading.

With the development of oil and gas exploration, oil industry researchers become interested in the deep-water regions. The Zhu II depression that presents high oil potential, and specifically the Baiyun Sag, attract some major attention. Pang et al. (2004) suggested that thermal subsidence of the Baiyun Sag led to a huge thick Cenozoic deposition of detrital matter, thus the sag became a subsidence and deposition center since the margin breakup. The mechanisms of long-term deposition and localization of subsidence center in the same sag remain enigmatic.

In this paper, we develop simple numerical models of subsidence behavior of the wide northern margin of the South China Sea. Our approach is based on a temperature dependent visco-elasto–plastic thin plate model (Burov and Diament, 1992). To construct our model, we use four long deep seismic sections across the northern margin of the South China Sea, such as the ESP-W, ESP-E (Nissen et al., 1995a; Yao et al., 1994), the OBH (Qiu et al., 2001) and the OBS93 (Yan et al., 2001) (Figs. 2 and 3), of which, only Profile OBS93 crosses the Baiyun Sag. Based on the crustal structures derived from these data, we attempt to provide new insights in the mechanisms of the subsidence phenomena, lithospheric strength and nature of the high velocity layer in this region.

2. Geological background

The northern margin of the South China Sea constitutes a wide rifted continental margin (Fig. 2) that spreads for 400 km between the limits of the unstretched crust and the continent–ocean boundary (COB). Since the Late Cretaceous, the northern margin has experienced multi-episodic rifting (Ru and Pigott, 1986), and evolved into a small "Atlantic", non-volcanic (Yan et al., 2001; Qiu et al., 2003)

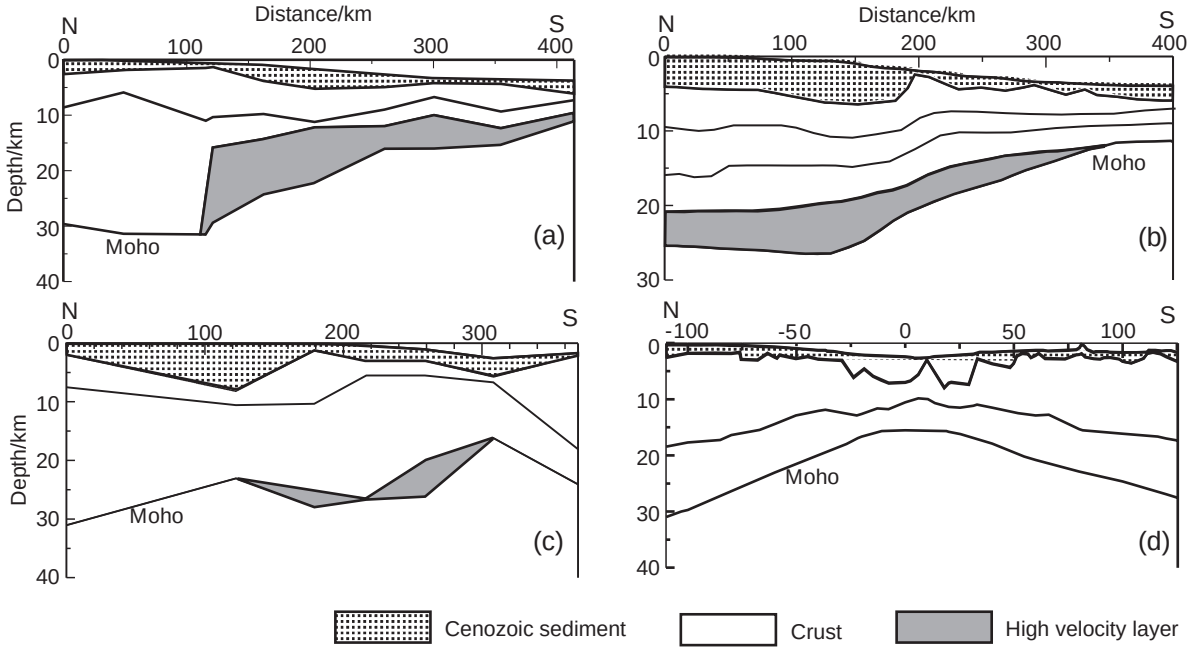

Fig. 3. Four deep seismic structure profiles (a, ESP-E; b, OBS93; c, ESP-W and d, OBH) whose locations are shown in Fig. 2.

passive continental margin during seafloor spreading of the South China Sea from 32 to 15.5 Ma (Taylor and Hayes, 1983; Briais et al., 1993). Since then it has experienced widespread thermal subsidence, emphasized by variation of heat flow along the northern margin of the South China Sea that increases from 61 mW/m^2 on the shelf to 73–80 mW/m^2 in the slope area (Shi et al., 2003). As a result, two sub-basins and three rises trending NE–ENE, constitute the Pearl River Mouth Basin. From north to south, these structures consist of the Northern Fault Terrace, the Northern Subsidence Zone including Zhu I and Zhu III depressions, the Central Rise Zone including the Shenhu Rise, Panyu Low Rise and Dongsha Rise, the Southern Subsidence Zone including the Zhu II and Chaoshan depressions, which straddle the shelf and the slope, and the Southern Rise. These depressions have received large amounts of Cenozoic sediments. In the northern subsidence zone, the largest Cenozoic sediment thickness is up to 9 km in the Zhu III depression, thicker than the 7 km in the Zhu I Depression, while in the southern subsidence zone, the largest Cenozoic sediment thickness of the Baiyun Sag exceeds 10 km (Pang et al., 2004). After continental break-up and seafloor spreading in the late Oligocene, and the whole thermal subsidence of the northern margin since the Late Oligocene, seawater transgressed the Central Uplift Zone, and entered the northern subsidence zone in the Early Miocene. Since this time, the Central Uplift Zone has received marine sediments underlain by porous Upper Oligocene to Lower Miocene quartz sandstones, which, in turn overly the Mesozoic basement (Ludmann and Wong, 1999). In the Central Rise Zone, the Cenozoic sediment thickness is about 1–3 km, and increases towards the depressions.

On the northern margin, a high velocity layer with seismic velocities between 7.0 and 7.5 km/s has been revealed within the lower crust on Profiles ESP-E, OBS93 and ESP-W (Fig. 3), while Profile OBH, which crosses the failed rift Xisha Trough, shows no high velocity layer in its crustal structure. Profile ESP-W also crosses the Xisha Trough, but is closer to the broken margin.

Though it was considered to be non-volcanic passive margin for the lack of the landward flood basalts and seaward dipping reflectors (SDRs), the northern margin of the South China Sea has experienced multiple magmatic events during pre-rifting, rifting and post-rifting phases. During the Jurassic and Cretaceous (Yansanian) periods, Southeast China has experienced widespread magmatism. Cretaceous intrusive rocks are dominantly granite and formed in four major episodes during 136–146, 122–129, 101–109 and 87–97 Ma (Li, 2000). In the Pearl River Mouth Basin, there are more than 50 wells that have encountered Pre-Tertiary basement, and 90% of the rocks are Yansanian intermediate–acid igneous rocks, dated at 70.5–153 Ma (Li et al., 1998). During the Cenozoic, there are also multiple magma activities. 16 wells have encountered Cenozoic volcanic rock and tuff in the Pearl River Mouth Basin, dated at 57.1–17.1 Ma (Li and Rao, 1994). Combined with seismic profiles, where seamounts can be identified, Li and Rao (1994) divided the Cenozoic magmatism into three stages, Late Paleocene–Oligocene (57.1–27.17 Ma), mainly intermediate–acid rock, Early Miocene (24.3–17.1 Ma), mainly basalt, and Post-Miocene, mainly basalt, with the occurrence of seamounts.

3. Tectonic subsidence

The Baiyun Sag, the main sag of the NE–SW trending Zhu II Depression is conventionally subdivided into three "subsags": Baiyun Main Subsag, Baiyun West Subsag and Baiyun East Subsag. The abnormal short-time high depositional rates have been observed in seven commercial wells around the Baiyun Sag (Fig. 2) and seismic sections (Wang, 2001), which indicates that there was a very short period (around 17 Ma) during which the deposition was very intensive. Thickness of sediments accumulated during this period varies from 720 to 241 m (uncompacted), with an average thickness of 452 m. The average thickness of deposits in the four wells located on the northern slope of the Baiyun Sag is larger (574 m) than the thickness observed in the three western wells. According to seismic data, the largest sedimentary thickness during this period corresponds to the center of the sag and may reach up to 1200 m (Wang, 2001).

Of course, high deposit rate does not necessarily mean high tectonic subsidence. Sediment deposition rates may change because of far-field variations in sediment supply, sea level or even delta lobe switch-

ing. In order to derive tectonic subsidence from well-log information, the effect of compaction, sedimentary loading, water depth, and sea level variations during deposition must be treated with great precautions (Sclater and Christie, 1980). The first order estimates for tectonic subsidence can be estimate from reconstructions of sedimentary cross-sections at different times using backstripping techniques. Assuming that the lithosphere has negligible strength, the subsidence, Y, of water-loaded basement at time t is given by:

$$Y = S\left(\frac{\rho_m - \rho_s}{\rho_m - \rho_w}\right) - SL\left(\frac{\rho_m}{\rho_m - \rho_w}\right) + W_d \qquad (1)$$

where S is the sediment thickness at time t which certainly have been decompacted when backstripped. ρ_m, ρ_w and ρ_s are the densities of the mantle, water and decompacted sediment (average density), respectively. SL is the height of mean sea level above (or below) the reference surface. W_d is the water depth at time t (Steckler and Watts, 1978; Watts, 2001). Eq. (1) indicates that the tectonic subsidence rate depends not only on the variations of S, ρ_s, but also that of SL and W_d.

For decompaction, the variation of porosity ϕ is taken to be a simple exponential decay with increasing depth z, $\phi(z)=\phi_0 \exp(-cz)$, where ϕ_0 is the initial porosity at surface, and c is the compaction factor. Following Su et al. (1989) and Clift and Lin (2001), we used commonphysical parameters (grain density, initial porosity and compaction factor) of different sediment types (Sclater and Christie, 1980). The contents of sandstone, shalely sandstone, shale and chalk are estimated according to the lithological description of well logs. The second order sea level reconstruction of Haq et al. (1987) was used to estimate the global eustatic sea level. The paleo-bathymetry was estimated using the data of lithological paleo-geography (Wang, 2001). Another important parameter influencing the shape of tectonic subsidence curves is the age of the strata. With the accumulation of various kinds of data including fossils data and data of sequential stratigraphy, the dating of the post-rift sediments is now well-constrained, and can be compared with the results of ODP Site 1148 on the continental slope offshore the Pearl River Mouth Basin. Six dated sequences stratigraphic packages of 21 (now is thought to be 23.8 Ma)–17.5 Ma, 17.5–16.5, 16.5–15.5, 15.5–13.8, 13.8–12.5 and 12.5–10.5 Ma have been recognized (Pang et al., 2004). Within the syn-rift deposits, there are several unconformities, and their ages, however, are poorly defined.

The tectonic subsidence curves of Wells PY33-1-1 and LH9-4-1 are shown in Fig. 4, which indicates that, around 17 Ma, corresponding to the high deposit rate, there was a quick tectonic subsidence, and that these subsidence rates are much larger than possible thermal subsidence rate estimated from common pure shear models (Jarvis and McKenzie, 1980). This

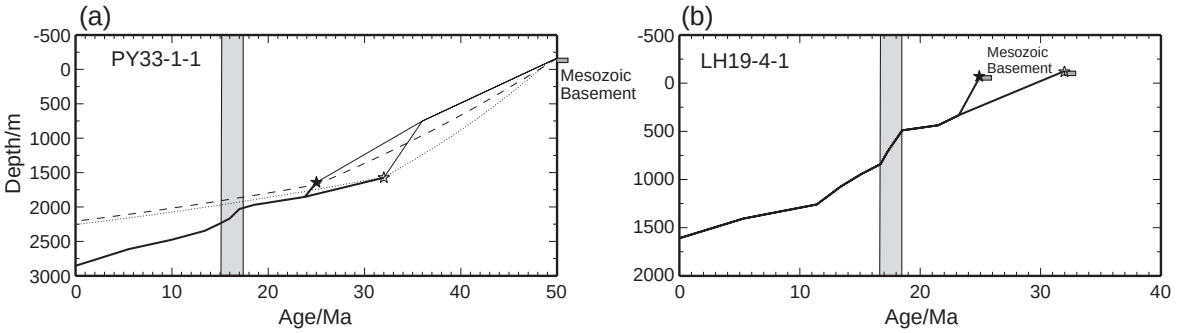

Fig. 4. (a) Observed and theoretical tectonic subsidence curves for Well PY33-1-1. Since the basement is not reached by Well PY33-1-1, thin solid line presents tectonic subsidence based on the strata thickness estimated from seismic data. Thick solid line is the tectonic subsidence based on the well log data. Theoretical tectonic subsidence curves, calculated with the finite extension model by Jarvis and McKenzie (1980), are shown with short dashed line (for stretching factors $\beta=1.9$, crustal thickness $T_c=30$ km, the duration of the stretching Δt is 18 my), and with long dashed line (for $\beta=1.9$, $T_c=30$ km, and Δt 25 my). (b) Observed tectonic subsidence curve for Well LH19-4-1 whose strata ages are mainly based on foraminifer (Lin et al., 2004). The solid star and the open star represent the same surface, i.e., the breakup unconformity, but assigned to two different ages (solid star for 25 Ma, and open star for 32 Ma), since the age for the breakup unconformity (probably ranging from 32 to 25 Ma) is not certain.

short-term quick subsidence suggests that during this period, this region could experience another rifting phase, just as suggested by Clift and Lin (2001) and Lin et al. (2003) for the young quick subsidence events revealed on the northern margin of the South China Sea. Such a quick subsidence could also be caused by a quite specific event such as a dense intrusion.

4. Necking method and results

To investigate the factors that could have contributed to the subsidence of the Baiyun Sag, we used a thin plate model of the lithosphere. During the rifting phase, localized thinning (necking) occurs around the level of maximum strength of the lithosphere (called "depth of necking", Z_{neck}) (Braun and Beaumont, 1989) that remains roughly horizontal. If Z_{neck} is deeper than the CD (compensation depth). In this case the restoring isostatic force is directed upward and tends to return the lithosphere to the level of the CD. However, the strength of the lithosphere prevents this process, which results in formation of an overdeepened basin. When Z_{neck} is shallower than the CD, the resulting basin is "underdeepened" (Kooi and Cloetingh, 1992; Keen and Dehler, 1997). For different stretching factors, various combinations of Z_{neck} and T_e will generate different basement topographies. Therefore, our main goal here is to find an optimal combination of Z_{neck} and T_e that will provide the best fit to the basement topography. The initial subsidence S immediately after rifting can be estimated as (Weissel and Karner, 1989):

$$S = \gamma Z_{neck} \tag{2}$$

where $\gamma = 1 - (1/\beta)$ is the crustal thinning factor (Davis and Kusznir, 2002), and β is the stretching factor (McKenzie, 1978). β is defined as the ratio of the initial crustal thickness to the observed crustal thickness. This initial basement subsidence is subsequently flexurally modified due to the presence of a vertical load. Because we have no detailed time-dependent data for the loading history, we follow the approach of Keen and Dehler (1997) that consists in subtraction of the effect of the present total vertical load to estimate the depth of basement before loading. This depth is obtained assuming that the initial subsidence S is superimposed on the flexural deflection $w(x)$:

$$\frac{d^2}{dx^2}\left(D(x)\frac{d^2w(x)}{dx^2}\right) + \frac{d}{dx}\left(T(x)\frac{dw(x)}{dx}\right) + \rho_m g w(x) = q(x) = q_{sw} + q_c + q_m - q_0 \tag{3}$$

where x is horizontal coordinate, D is flexural rigidity, $D(x) = ETe^3(x)/12(1-\nu^2)$, where E is Young modulus and ν is coefficient of Poisson, T is fiber force, g is acceleration due to gravity, q_{sw} is the normal load including sediment and seawater load above the actual basement, q_c is the load due to thinned crust estimated as $\rho_c g\, T_c(1-\gamma)$, where ρ_c is the density of the crust, T_c is the initial crustal thickness. q_m is the load due to the mantle material replacing of the thinned crust from below (estimated as $\rho_m g\gamma(T_c - Z_{neck})$, q_0 is the weight of an isostatically compensated column referred to the depth of compensation in remote oceanic lithosphere. In this study, we ignore the horizontal force $T(x)$, and assume $E = 8\times10^{10}$ Pa, $\nu = 0.25$ (Burov and Diament, 1995).

Fig. 5 shows the crustal structure of the Profile OBS93 published by Yan et al. (2001). Based on this structure, we used the necking method to calculate the location of the basement under the loading. The results of Yan et al. (2001) indicate a high-velocity layer (V_p=7.1–7.4 km/s) lying in the lowermost crust and supposed to be the underplating material. The stretching factor β along the profile can be quite different whether or not the high velocity layer is a part of the initial crust (Fig. 5). If the high velocity layer was a part of the initial crust, the shape of the basement can be very different from the observed basement in the case of strong lithosphere (Fig. 6a), and as the strength decreases, the calculated basement approaches the prediction for t local compensation, which is close to the shape of the observed basement. If the high velocity layer was not a part of the initial crust, the shape of the calculated basement is similar to the observed basement even in the case of strong lithosphere. For this reason, the following experiments use larger β's. Except for the continental crust, the densities for different surface and subsurface units were deduced from direct gravity modeling. The density of the continental crust was set to 2800 kg/m^3, except for the experiments shown in Fig. 6(f).

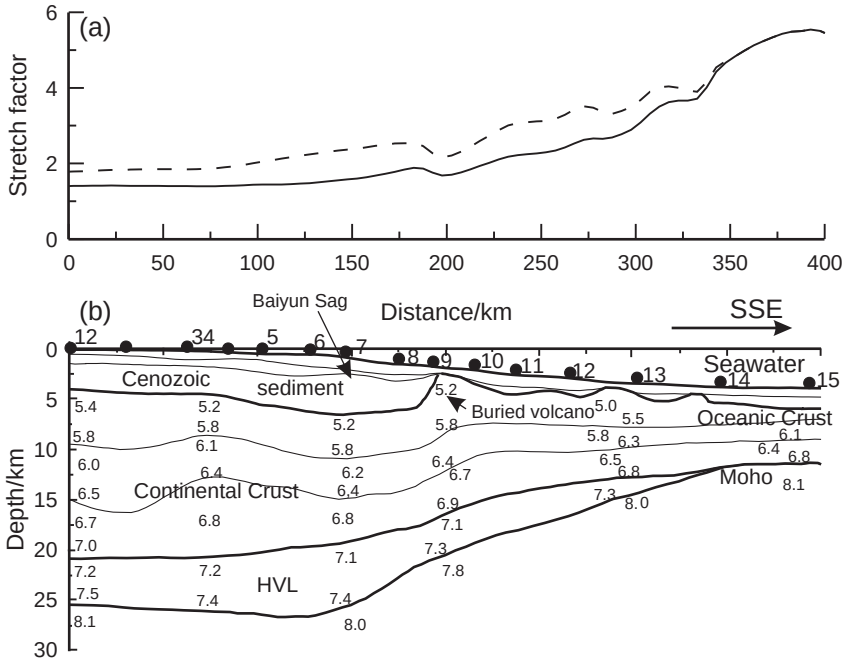

Fig. 5. (a) The stretch factor defined as the ratio between the initial crust thickness to the observed crust thickness including the high velocity layer (solid line) or not (dashed line) along Profile OBS93. (b) The simplified crustal structure of Profile OBS93 published by Yan et al. (2001), who recognized the buried volcano. The solid circles numbered represent the location of the OBSs and their numbers. Indicated velocities are in units of km/s.

For the case of local compensation, the model suggests that the location of the basement is the same for all tested parameter combinations and is shallower than the observed basement under the Baiyun Sag. Based on previous studies (e.g., Kooi and Cloetingh, 1992; Keen and Dehler, 1997), one can predict that deeper Z_{neck} will produce deeper basins, which is confirmed by the experiments shown in Fig. 6b. Assumption of a larger Z_{neck} can provide a good match with the observed basement, but the rift shoulders will be higher than actually observed. In fact, Z_{neck} depends on the rheological properties of the lithosphere, therefore on its thermal structure before rifting (Kooi and Cloetingh, 1992; Cloetingh et al., 1995). Since the South China and the northern margin of the South China Sea have experienced widespread thermal events, the assumption of a large Z_{neck} seems unreasonable. For a fixed value of Z_{neck}, the sag becomes wider and shallower with increasing T_e (Fig. 6c and d). If one assumes a thicker initial crust (and consequently larger β), the resulting basin will be shallower for the same Z_{neck} and T_e values, because of a larger upward restoring force (Fig. 6e). For the assumed density range, we could not match the observed basement of the Baiyun Sag. Even though one can increase the density of the continental crust, the assumption of higher density will result in mismatch between the predicted and observed basement in other areas (Fig. 6f). This suggests the existence of unaccounted denser bodies below the sag than country rock.

5. Gravity modeling

To test the presence of dense bodies, the satellite-derived marine free-air gravity anomalies along Profile OBS93 have been extracted from the data sets published by Sandwell and Smith (1997). The data along Profile OBH across the Xisha Trough are in good agreement with the free-air gravity data collected during SO49 cruise (Shi et al., 2002).

For the model, the Cenozoic sedimentary cover was sub-divided into two density units defined

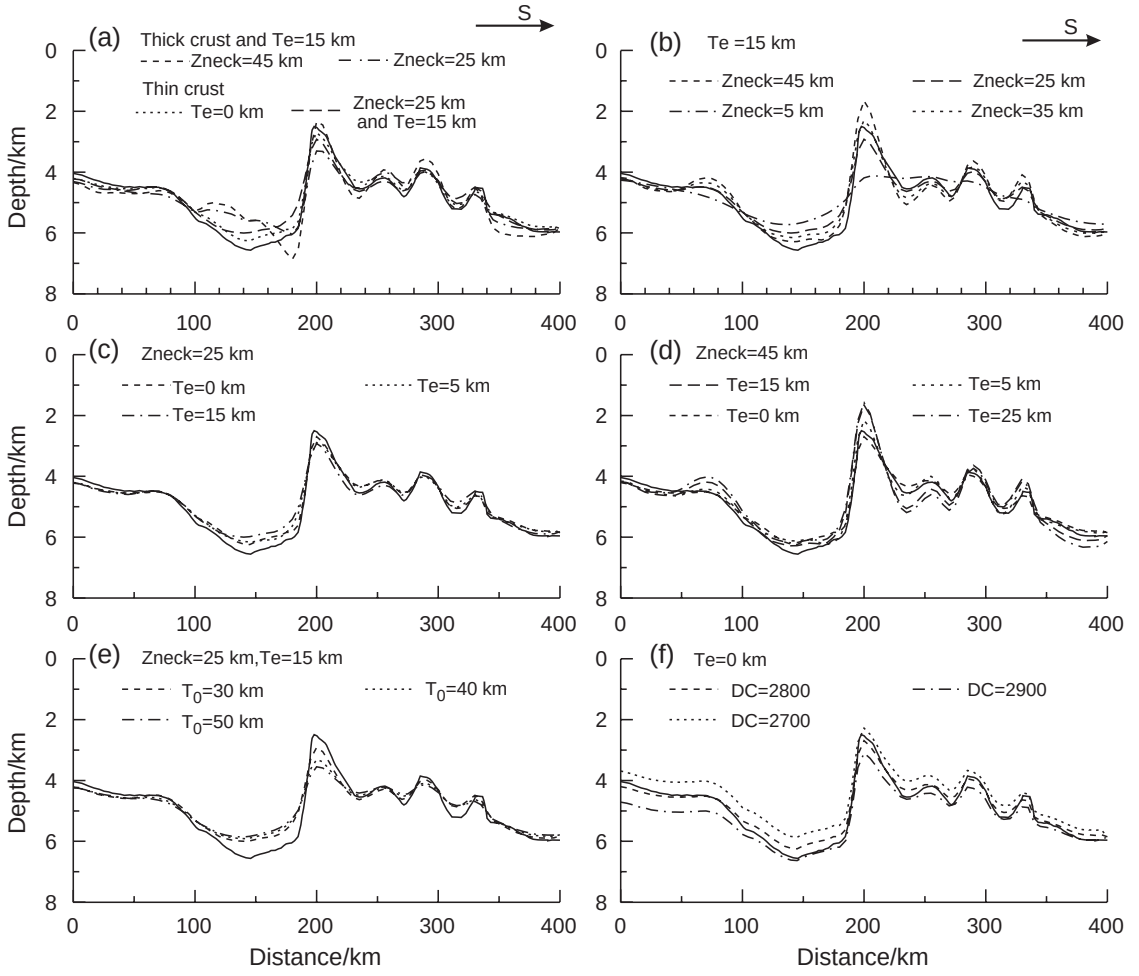

Fig. 6. (a) Calculated basement geometries for opposite cases as to the presence of the high velocity layer in the initial crust. Thick crust indicates that the high velocity layer is a part of the initial crust, while thin crust indicates that the high velocity layer is not a part of the initial crust. (b) Calculated basements for different values of Z_{neck} (45, 35, 25 and 5 km) when T_e=15 km. (c) Calculated basements for Z_{neck}=25 km and different T_e values (0, 5 and 15 km). (d) Calculated basements for Z_{neck}=45 km and different T_e (0, 5, 15 and 25 km). (e) Computed basements for different initial crustal thickness T_o (30, 40 and 50 km). (f) Local compensation assuming different crustal densities CD. Indicated densities are in units of kg/m^3. Solid line represents the observed basement.

according to the seismic structure shown in Fig. 5. The crust was initially divided into three horizontal layers based on the velocity model of Yan et al. (2001). A simple eight-unit density–depth model, involving a water layer, two units for Cenozoic sediments, upper crust, middle crust, lower crust, high velocity layer and upper mantle was used assuming densities converted from the velocity model using the velocity vs. density relationship of Ludwig et al. (1970). To avoid edge effects, the profile has been extended for more than 200 km from each side. The forward modeling (Figs. 5–7) is based on a semi-automatic 2.5D gravity and magnetic modeling program, ‘‘Saki’’ from the U.S. Geological Survey. The preferred density structure is shown in Fig. 7.

The gravity modeling suggests that the observed gravity anomaly cannot be explained by a simple layered density structure. The best fitting model requires laterally varying density structure, increased density of the basement (2700 kg/m^3) under the Baiyun Sag, and lower densities of the surrounding blocks (2600 kg/m^3). Yan et al. (2001) have identi-

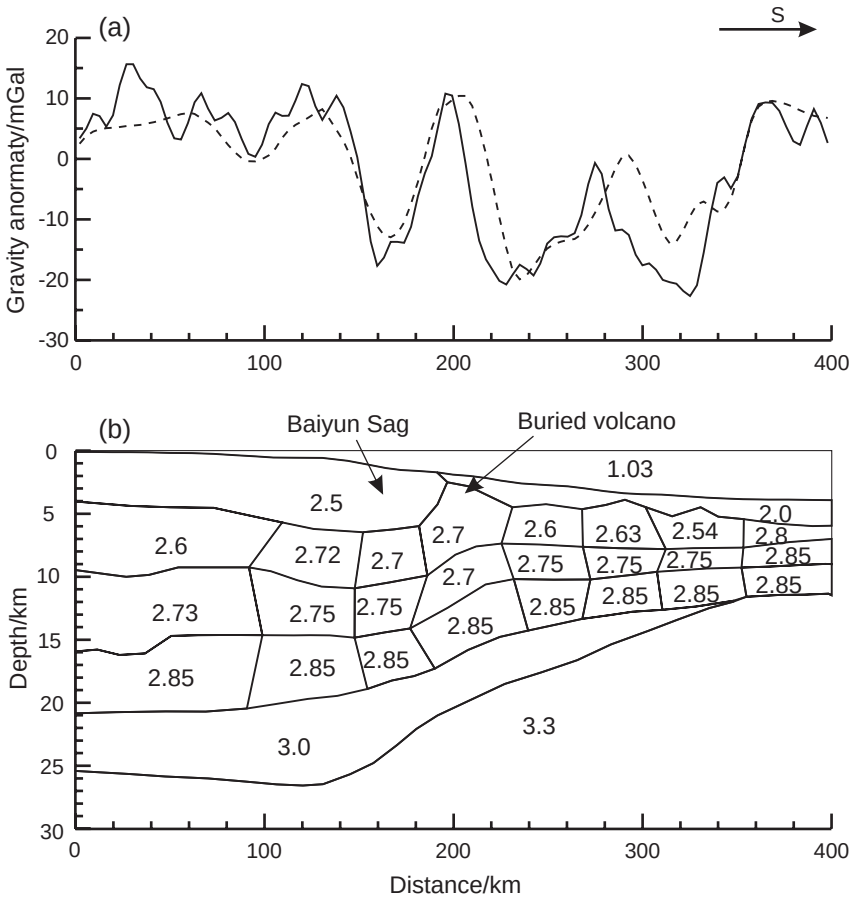

Fig. 7. (a) Observed (solid line) and calculated (dashed line) free-air gravity anomaly. (b) Density–depth structure of Profile OBS93. Indicated densities are in units of 10^3 kg/m^3.

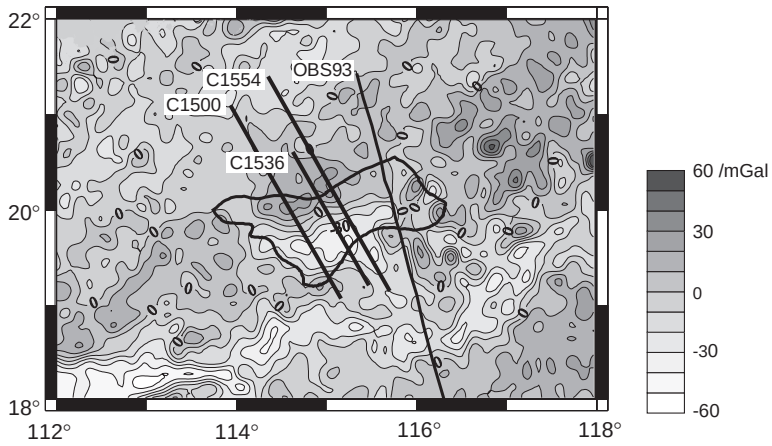

Fig. 8. Satellite-derived marine free-air gravity anomaly map of the Baiyun Sag (thick solid curve) and surrounding area. Profiles OBS93, C1554, C1536, C1500 are shown with thick solid lines.

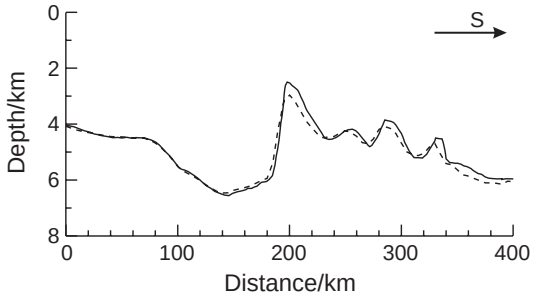

Fig. 9. The observed (solid line) and computed (dashed line) basement (assumption of local isostasy).

fied a buried volcano in the basement high at the south of the Baiyun Sag (Fig. 5). The results of Wang et al. (1997), who modeled profiles 1500 and 1554 (see Figs. 2 and 8 for locations) across the Baiyun Main Subsag using free air gravity and magnetic anomaly data jointly, show that the basement of the Baiyun Main Subsag also consists of denser materials with densities ranging from 2800–2860 kg/m^3 under the sag, while the densities of the southern and northern basement range from 2530 to 2650 kg/m^3. Combined with the analysis of magnetic data, Wang et al. (1997) suggested that the dense materials correspond to a combination of granite and basalt. The gravity anomaly of the Baiyun Sag (Fig. 8) consists of the northern gravity high zone and the southern low zone with the same trend as the sag, while the dense bodies discovered by Wang et al. (1997) and in our study lie underneath the gravity anomaly characterized by gradual change of the amplitude from high positive values at the north to low negative values at the south. This suggests a presence of a large continuous dense zone under the sag that has the same trending as the sag. We note that the densities of Wang et al. (1997) are higher than our estimates, which can be explained by differences in the methods used, but also by different proportion of basalts below the Main Subsag, which may be higher than for the Eastern Subsag (Profile OBS93). Based on the above-derived density structure and using the necking method, we recomputed the theoretical basement location for Profile OBS93 (Fig. 9). We found that under the assumption of local isostasy, the calculated basement geometry could match the observed one as well, which also signifies that the lithosphere under the Baiyun Sag may have very low strength.

6. Thermal and subsidence model

Though it is impossible to determine the time when the dense intrusion was emplaced into the crust, it is important to constrain the extent and duration of the impact of this intrusion on the subsidence of the sag if the emplacement took place during the formation of the basin. To answer this question, we employed a simplified thermal model, where we assumed that the lithosphere was stretched instantaneously at 60 Ma with stretching factor defined as the ratio of the initial crustal thickness (30 km) to the present crustal thickness. The lithosphere is allowed to cool down during the period

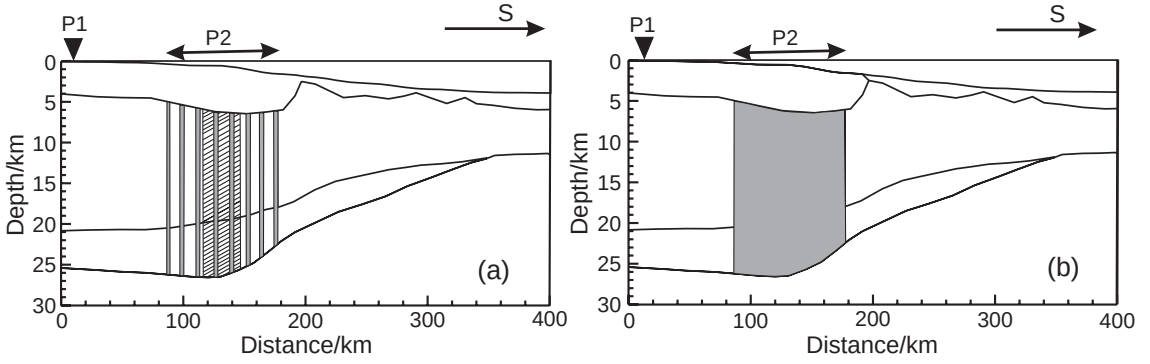

Fig. 10. (a) The assumed 30 km wide basaltic dike material is evenly distributed over a 90 km wide crustal column. For convenience, the 30 km wide dike with initial temperature 1000 °C was emplaced in the middle of the region at 17 Ma. (b) The entire 90 km wide shaded crustal column is emplaced by dike. P1 and P2 are the locations for subsidence curves shown in Fig. 11.

Table 1
Parameters used in the thermal and subsidence model

Symbol	Value
Model thickness, a	100 km
Temperature of the asthenosphere, T_1	1300 °C
Thermal conductivity, k	2.5 Wm/°C
Volumetric heat capacity, $\rho \times c$	2.5×10^6 J/mK
Cenozoic sediment density, ρ_s	2.5×10^3 kg/m^3
Upper crust density (at 0 °C), ρ_{c1}	2.6×10^3 kg/m^3
Middle crust density (at 0 °C), ρ_{c2}	2.7×10^3 kg/m^3
Lower crust density (at 0 °C), ρ_{c3}	2.85×10^3 kg/m^3
High velocity layer density (at 0 °C), ρ_{c4}	3.0×10^3 kg/m^3
Mantle density, ρ_{cm}	3.0×10^3 kg/m^3
Basalt density (at 0 °C), ρ_{cb}	2.95×10^3 kg/m^3

between 60 and 17 Ma, since the abnormal quick subsidence took place around 17 Ma, and we thought it was related with an intrusion event (see Discussion and conclusion). At the end of this period, we introduce an instantaneous hot basalt intrusion into the model and let the thermal relaxation to continue. The density of the igneous basalt is about 2950 kg/m^3 (Turcotte and Schubert, 1982), while the densities of the country rock and of the dense body are about 2600 and 2700–2720 kg/m^3, respectively (Fig. 7b). Therefore, we assume that the dense body is composed of the igneous basalt and of the country rock in the proportion 1:2, so the igneous basalt could have contributed to about a third of the 90 km wide dense body (Fig. 7, not including the southern buried intrusion, which has been thought to be emplaced lately (Yan et al., 2001) (Fig. 10a). The assumed total width of the imposed central basaltic dike is thus 90:3=30 km.

In the thermal model, we employed a 2D unsteady thermal diffusion equation:

$$\rho c \frac{\partial T}{\partial t} = k\left(\frac{\partial^2 T}{\partial x^2} + \frac{\partial^2 T}{\partial x^2}\right) \tag{4}$$

where ρ is the density of the rock, c is specific heat, T is temperature, t is time, k is thermal conductivity. Parameters used in the thermal and subsidence model are shown in Table 1.

The initial and boundary conditions are similar to the uniform extension model (McKenzie, 1978). We assumed that the following initial conditions:

$$\begin{aligned} T(x,z) &= T_1 \qquad 0<z(x)<z_0(x) - \alpha/\beta(x) \\ &= \frac{\beta(x) T_1}{a}(z_0(x) - z(x)) \\ z_0(x) - \alpha/\beta(x)<z(x)<z_0(x) \end{aligned} \tag{5}$$

where z is depth measured upward from the base of lithosphere assumed to be 100 km thick; $z_0(x)$ is the location of the upper surface. Because the exact time of intrusion is unknown, we ignore the related sedimentation, so $z_0(x)$ corresponds to the depth of the basement. The boundary conditions are:

$$T(x, z_0(x)) = 0$$

$$T(x, 0) = T_1$$

For convenience, the imposed 30 km wide dike with initial temperature 1000 °C was emplaced in the center of the dense region at 17 Ma (Fig. 10). It is noteworthy that the simplified model conditions cannot exactly reproduce the observations. Our model did not include some detailed features such as, multi-episodic rifting (Ru and Pigott, 1986; Zhou et al., 1995a,b; Clift and Lin, 2001) and the margin breakup at about 30 Ma. Our purpose, however, was designed primarily to understand for how long the basalt intrusion could disturb the temperature field, and thus to evaluate the temporal influence of the intrusion event on the crustal subsidence. Fig. 11a shows the calculated temperature field at different times. As can be seen, the thermal perturbation produced by the intrusion rapidly decreases, so that its influence on the temperature field is important only during the first 5 my following the intrusion. 10 my after the intrusion, the perturbation becomes negligible. We also consid-

Fig. 11. (a) The temperature fields at different times before and after the intrusion of a 30 km-wide 1000 °C dike, without Cenozoic sediment in the case of Fig. 10a, and the water-loaded subsidence of P1 and P2. (b) The temperature fields 5 my after the intrusion of 90 km-wide 1000 °C dike, without Cenozoic sediment (in the case of Fig. 10b), and the water-loaded subsidence of P1 and P2. (c) The temperature fields at 0.1, 5 and 10 my after the intrusion of 90 km-wide 1000 °C dike, with Cenozoic sediment, and the water-loaded subsidence of P1 and P2. The dashed-dotted line is the calculated subsidence curve of P1, and the solid line is the average subsidence of the 90 km wide column P2, the dashed line shows the subsidence of P2 if without intrusion. The locations of P1 and P2 are shown in Fig. 10.

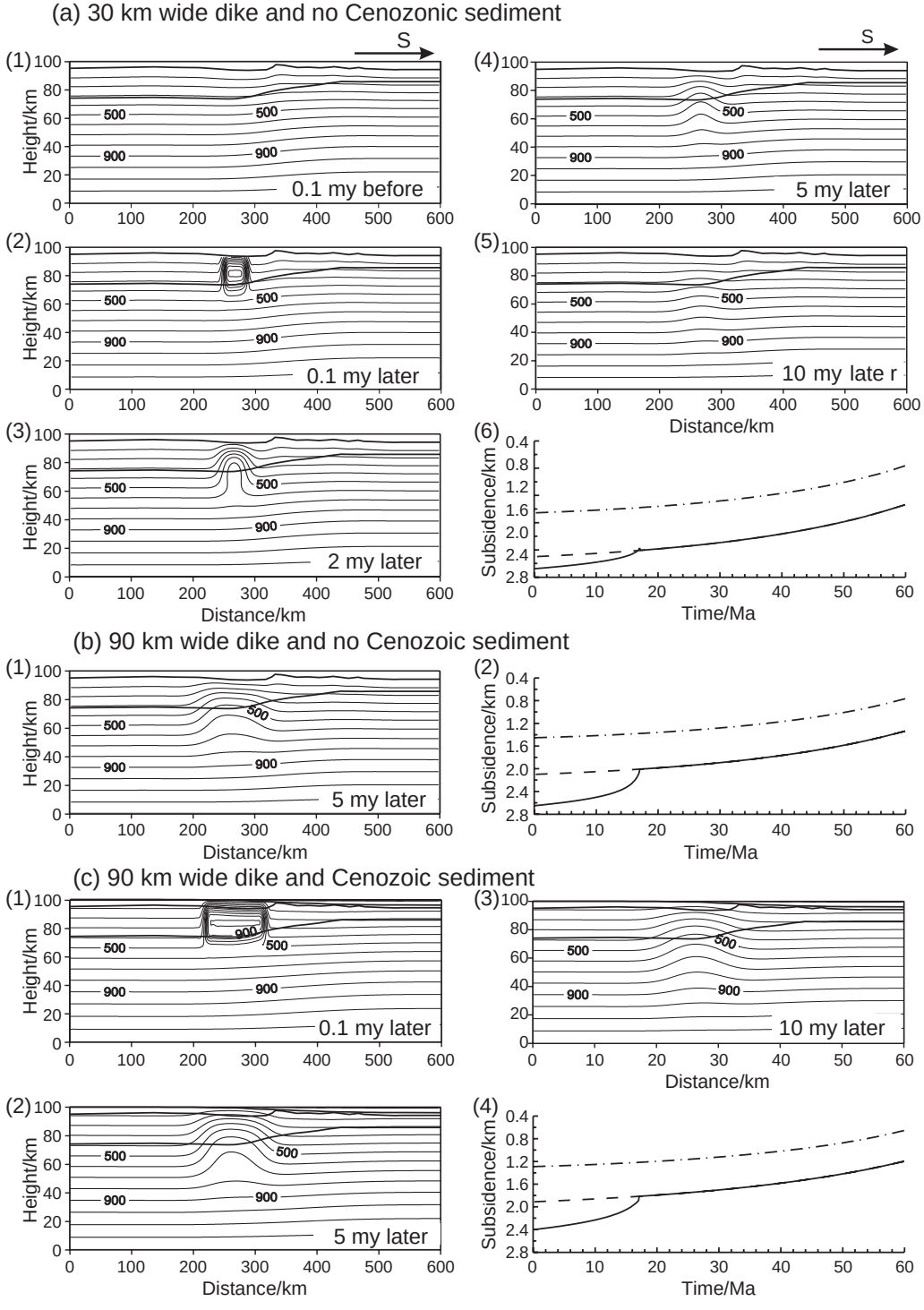
(a) 30 km wide dike and no Cenozonic sediment
(1)
(2)
(3)
(4)
(5)
(6)
S
0.1 my before
0.1 my later
2 my later
5 my later
10 my late r
Height/km
Distance/km
Subsidence/km
Time/Ma
500
900
(b) 90 km wide dike and no Cenozoic sediment
5 my later
(c) 90 km wide dike and Cenozoic sediment
0.1 my later
10 my later
5 my later

ered the case with a 90 km-wide dense body representing a large basalt dike (Figs. 10b and 11b). The result is similar to the previous experiment. The excess heat decays mostly in the first 5 my after intrusion. Some differences exist in the case when the basement is covered by Cenozoic sediments (Fig. 11c). Since we do not have any quantitative information on sedimentary deposition and timing of the basalt intrusion, we simply assume that the dike was covered by Cenozoic sediments, which should have strengthened the effect of thermal blanketing. Because of the thermal blanketing by the sedimentary cover, the heat decay is delayed but, nevertheless, after 10 my, the influence of the dike on the temperature field becomes negligible.

We have computed the average water-loaded subsidence for the dense body (90 km in width) caused by 30 km wide and 90 km wide intrusions (Fig. 10) under the assumption of Airy isostasy. The density structure (Fig. 7b) shows that the significant difference between the intrusion and country rock lies in the upper crust, therefore, the following calculated subsidence (Fig. 11) was primarily caused by the emplacement into the upper crust. Fig. 11 indicates that the subsidence should be very rapid immediately after the intrusion during the first 5 my, and then it slows down. The real subsidence rate may depend on the time-dependent response of the lithosphere. The average subsidence caused by the intrusion can reach 180 m (in the case of Fig. 11a), 490 m (Fig. 11c) and 520 m (Fig. 11b). If all space available for deposition was filled by sediment with density of 2.5×10^3 kg/m^3, the sediment thickness caused by the intrusion would be 500–1500 m. Thermal blanketing, which may delay the subsidence, has little effect on the subsidence rate (Fig. 11b). When the subsidence is caused by the emplacement in the whole crust, not just in the upper crust, the subsidence would be much larger, and even the air-loaded subsidence can reach 270 m (in the case of Fig. 11a) or 830 m (in the case of Fig. 11b).

7. Discussion and conclusion

The abnormal short-time high depositional rate and quick subsidence took place (Fig. 4) in the Baiyun Sag around 17 Ma. Gravity modeling also reveals a dense body in the basement of the Baiyun Sag (Fig. 7; Wang et al., 1997), which is also confirmed by our necking model (Fig. 6). Combined with magnetic and gravity modeling, Wang et al. (1997) suggested that the dense body correspond to a combination of granite and basalt. The dense body could not be detected directly from seismic observations (Fig. 5), most probably because of deep buried basement and low identification of wide angle profile.

Although it is impossible to tell exactly when the basalt was emplaced into the basement, the basic magmatism dated by 17 Ma was discovered in the area. Between 2401 and 2842 m in depth, except for thin stratified lime at the top and on the bottom, Well BY7-1-1, located near the Baiyun Sag, has encountered thick basalt and basalt ash tuff, and the K–Ar ages of the samples located at 2429 and 2432 m are 17.1 ± 2.5 and 20.2 ± 3.0 Ma, respectively (Li and Liang, 1994; Zou et al., 1995b). Wang (2001) suggested that some potential oil and gas bearing structures such as BY7-1 and BY6-1 were developed by the eruption of basic magma. Xia and Zhou (1993) identified a belt of high magnetic anomalies that appears in the Penghu Islands, the Dongsha Rise, the Zhu II Depression and continues westwards to the Shenhu Rise. These high magnetic anomalies are the indication for basic rocks, and in the Penghu Islands, alkali tholeiitic basalt and alkali basalt of 16.2–8.2 Ma have been observed (cf. Xia and Zhou, 1993; Yu, 1997). Ho et al. (2000) suggested that the Leiqiong area, which includes the Leizhou Peninsula and the northern part of the Hainan Island, was the largest province of exposed basalts in southern China. $^{40}Ar/^{39}Ar$ and K/Ar dating indicate that volcanism in the Leiqiong area may have taken place in late Oligocene and gradually increased in tempo toward the Miocene and Pliocene, and were most extensive during Pleistocene, and declined and ended in Holocene. These evidences show that during Miocene, there is no doubt that basaltic magmatism took place on the northern margin of the South China Sea. Though we cannot exclude that the short-term quick subsidence was caused by a possible new phase of extension, it would be difficult to circumvent the similarities between the observed subsidence curves (Fig. 4) and the predicted subsidence curves (Fig. 11) for intrusion. We believe that the emplacement of denser intrusion (Fig. 1b and c) may be responsible for some episodes of subsidence, perhaps for the episode of quick sub-

sidence in the Baiyun area. Indeed, Ludmann et al. (2001) have suggested that the two uplift and erosion events on the Dongsha Rise (see Fig. 2 for location) that took place at the Miocene/Pliocene boundary and at the end of the lower Middle Pleistocene and were followed by subsequent quick thermal subsidence since the Last Glacial Maximum at an average rate of 15 m/ka, are due to magmato-tectonic events, similar to the model shown in Fig. 1c. Thus, the rapid subsidence observed at around 17 Ma in the Baiyun Sag could be linked to an intrusion event of dense material.

The subsidence caused by dense intrusion might be just an episode of the long-term subsidence history of the Baiyun Sag. Regional isostasy indicates that the sedimentary cover on the neighboring rises such as the Shenhu Rise and the Dongsha Rise may have increased the subsidence of the Baiyun Sag. However, the degree, in which the normal loading of the uplifted areas has contributed to the subsidence, depends on the strength of the lithosphere. The lithosphere under the northern margin of the South China Sea may be very weak. Our necking models suggest that the lithosphere under the Baiyun Sag has indeed a very low strength. Clift et al. (2002), who employed a flexural cantilever model, have suggested a quite low flexural rigidity so that T_e in the northern margin of the South China Sea probably did not exceed 3–5 km during the main Oligocene phase of extension. Bellingham and White (2000) also found that the smallest misfit between the observed and calculated stratigraphic record can be obtained for T_e less than 2 km. Lin and Watts (2002) employed a direct flexural model to estimate the flexural rigidity of the Taixi forland basin, and obtained a T_e value of 13 km for the area, and they attributed the low T_e values to the underlying passive margin sequence, which is affiliated with the northern margin of the South China Sea.

The high velocity layer in the lowermost crust is generally interpreted either as magmatic underplating resulting from partial melting of the upper mantle during rifting on the volcanic margins (e.g., White and McKenzie, 1989), or as partly serpentinized peridotites of the upper mantle exhumed in the continental breakup zone on non-volcanic passive margins (such as West Iberia margin, Whitmarsh et al., 2001). On the northern margin of the South China Sea, the high velocity layer has been discovered from the shelf to the slope along the seismic lines ESP-E, ESP-W and OBS93 (Figs. 1 and 3). Our necking models suggest that if the high velocity layer was a part of the initial crust, the shape of the basement could be very different from the observed basement in the case of strong lithosphere (Fig. 6a), whereas if the high velocity layer was not a part of the initial crust, the shape of the calculated basement would be similar to the observed basement even in the case of strong lithosphere. Nevertheless if the lithosphere has a negligible strength, the predicted basement topography is similar in both cases to the observed basement. Unfortunately, the lithosphere in the study area is so weak that necking models cannot effectively discriminate between the two cases. We prefer to the case in which the high velocity layer is not a part of the initial crust because in this case the predicted basement topography is similar to the observed basement independently of whether the lithosphere is strong or not. In this case, there is no high velocity layer in the lowermost crust along the Profile OBH (Figs. 1 and 3; Qiu et al., 2001), which indicates that not all the crust on the northern margin of the South China Sea has a high velocity layer in their lower part, and that the high velocity layer may not be an original part of the crust. The most likely explanation for the development of the high velocity layer on the northern margin of the South China Sea seems to be magmatic/underplating (Yan et al., 2001), rather than serpentinized peridotites. First, the typical serpentinized peridotites observed at the West Iberia Margin correspond to the continent/oceanic transition, while the high velocity layer has also been discovered on the shelf of the northern margin of the South China Sea. Second, the development of the latter would need great amounts of water and lower temperature conditions. Indeed, the thickness of the crust overlying the high velocity layer on the shelf is larger than 10 km, which makes it difficult for large volume of water to pass through (Yan et al., 2001). If the high velocity layer were due to underplating, this would have disturbed the isostatic balance of the region, leading to a buoyancy-driven uplift (Fig. 1a; Watts, 2001). For example, Mjelde et al. (2002) suggested that the high velocity layer on the VØring Margin was intruded during the last rift phase Late Paleocene/Early Eocene rift period. During this period, the initial subsidence was

followed by 1.2 km uplift and erosion, and the break up occurred here in Early Eocene. On the northern margin of the South China Sea, a great amount of intrusion (underplating) may have caused widespread uplift and an erosion event. In our case, the margin scale uplift event, and the related unconformity present a breakup unconformity event developing during the continental margin breakup (Ru and Pigott, 1986; Zhou et al., 1995a,b). This suggests that the widespread underplating took place in the period of margin breakup. The facts that the profile OBH (Figs. 1 and 3) that crosses the failed rift, the Xisha Trough, has no high velocity layer in its lower crust, and that the profile ESP-W (Figs. 1 and 3) that also crosses the Xisha Trough, but closer to the broken margin, has a much thinner high velocity layer than the two profiles ESP-E and OBS-93 (Figs. 1 and 3), which cross the broken continental margin, also support the idea that the high velocity layer was emplaced when the margin broken up. The large scale intrusion (underplating), but without seaward dipping reflector sequences (SDRS), is a characteristic feature of the northern margin of the South China Sea. The mechanism for these phenomena is, however, still not clear. Based on the presence of igneous activity, passive continental margins are generally classified either as volcanic or non-volcanic. However, the divide between these two end members may not be as distinct as it is commonly assumed, and there may be some transitional margins just like the one observed on the northern margin of the South China Sea (Clift et al., 2001).

Acknowledgements

Figs. 1 and 8 were plotted with GMT (Wessel and Smith, 1995). We thank two anonymous reviewers for their thorough critical comments and helpful suggestions on the manuscript. Their reviews substantially improved the paper. This work was supported jointly by the National Natural Science Foundation of China (Grant 40204006), the Chinese Academy of Sciences (Grants KZCX2-SW-117, KZCX3-SW-234-3), the Chinese Ministry of Science and Technology (Grant G2000-046-701). Dr. Xiaobin Shi gratefully acknowledges the support of K.C. Wong Education Foundation, Hong Kong, and Laboratoire de Tectonique, Universite de Pierre et Marie Curie, Paris.

References

Bellingham, P.B., White, N., 2000. A general inverse method for modeling extensional sedimentary basins. Basin Research 12, 219–226.

Braun, J., Beaumont, C., 1989. A physical explanation of the relation between flank uplifts and the breakup unconformity at rifted continental margins. Geology 17, 760–764.

Briais, A., Patriat, P., Tapponnier, P., 1993. Updated interpretation of magnetic anomalies and seafloor spreading stages in the South China Sea: implications for the tertiary tectonics of Southeast Asia. Journal of Geophysical Research 98 (B4), 6299–6328.

Burov, E.B., Diament, M., 1992. Flexure of the continental lithosphere with multilayered rheology. Geophysical Journal International 109, 449–468.

Burov, E.B., Diament, M., 1995. The effective elastic thickness (T_e) of continental lithosphere: what does it really mean? Journal of Geophysical Research 100 (B3), 3905–3927.

Chian, D., Louden, K.E., Reid, I., 1995. Crustal structure of the Labrador Sea conjugate margin and implications for the formation of nonvolcanic continental margins. Journal of Geophysical Research 100, 24239–24253.

Chery, J.F., Lucozeau, F., Daignieres, M., Vilotte, J.P., 1992. Large uplift of rift flanks: a genetic link with lithospheric rigidity? Earth and Planetary Science Letters 112, 195–211.

Clift, P., Lin, J., 2001. Preferential mantle lithospheric extension under the South China Sea. Marine and Petroleum Geology 18, 929–945.

Clift, P.D., Lin, J.ODP Leg 184 Scientific Party, 2001. Patterns of extension and magmatism along the continent–ocean boundary, South China margin. In: Wilson, R.C., et al., (Eds.), Non-volcanic Rifting of Continental Margins: A Comparison of Evidence from Land and Sea, Geological Society of London, Special Publication, vol. 187, pp. 489–510.

Clift, P., Lin, J., Barckhausen, U., 2002. Evidence of low flexural rigidity and low viscosity lower continental crust during continental break-up in the South China Sea. Marine and Petroleum Geology 19, 951–970.

Cloetingh, S., Van Wees, J.D., Van der Beek, P.A., Spadini, G., 1995. Role of pre-rift rheology in kinematics of extensional basin formation: constraints from thermomechanical models of Mediterranean and intracratonic basins. Marine and Petroleum Geology 12 (8), 793–807.

Davis, M., Kusznir, N., 2002. Are buoyancy forces important during the formation of rifting margins? Geophysical Journal International 149, 524–533.

Haq, B.U., Hardenbol, J., Vail, P.R., 1987. Chronology of fluctuating sea levels since the Triassic (250 Myr ago to present). Science 235, 1156–1167.

Ho, K., Chen, J., Juang, W., 2000. Geochronology and geochemistry of Late Cenozoic basalts from the Leiqiong area, southern China. Journal of Asian Earth Sciences 18, 307–324.

Jarvis, G.T., McKenzie, D.P., 1980. Sedimentary basin formation with finite extension rates. Earth and Planetary Science Letters 48, 42–52.

Keen, C.E., Dehler, S.A., 1997. Extensional styles and gravity anomalies at rifted continental margins: some north Atlantic examples. Tectonics 16 (5), 744–754.

Kooi, H., Cloetingh, S., 1992. Lithospheric necking and regional isostasy at extensional basins: 1. Subsidence and gravity modeling with an application to the Gulf of Lions Margin (SE France). Journal of Geophysical Research 97 (B12), 17553–17571.

Li, X., 2000. Cretaceous magmatism and lithosphere extension in southeast China. Journal of Asian Earth Sciences 18, 293–305.

Li, P.L., Liang, H.X., 1994. Relation between Cenozoic igneous activity and basin evolution and oil–gas accumulation in Pearl River Mouth Basin. Guangdong Geology 9 (2), 23–34 (in Chinese).

Li, P., Rao, C., 1994. Tectonic characteristics and evolution history of the Pearl River Mouth Basin. Tectonophysics 235, 13–25.

Li, P., Liang, H., Dai, Y., 1998. Exploration perspective of basement hydrocarbon accumulations in the Pearl River Mouth Basin. China Offshore Oil and Gas (Geology) 12 (6), 361–369 (in Chinese).

Lin, A.T., Watts, A.B., 2002. Origin of the west Taiwan basin by orogenic loading and flexure of a rifted continental margin. Journal of Geophysical Research 107 (B9), ETG2-1–ETG2-19.

Lin, A.T., Watts, A.B., Hesselbo, S.P., 2003. Cenozoic stratigraphy and subsidence history of the South China Sea margin in the Taiwan region. Basin Research 15, 453–478.

Lin, J., Zhang, J., Jiang, S., Wang, S., Xu, B., Wei, M., 2004. The Neogene foraminiferal stratigraphy of the LH-19-4-1 bore hole, Pearl River Mouth Basin, South China Sea. Journal of Stratigraphy 28 (2), 120–125 (in Chinese).

Ludmann, T., Wong, H.K., 1999. Neotectonic regime on the passive continental margin of the northern South China Sea. Tectonophysics 311, 113–138.

Ludmann, T., Wong, H.K., Wang, P., 2001. Plio–Quaternary sedimentation processes and neotectonics of the northern continental margin of the South China Sea. Marine Geology 172, 331–358.

Ludwig, W.J., Nafe, J.E., Drake, C.L., 1970. Seismic Refraction in the Sea: Part 1. New Concepts of Sea Floor Evolution, vol. 4. Wiley, New York.

McKenzie, D., 1978. Some remarks on the development of sedimentary basins. Earth and Planetary Science Letters 40, 24–32.

Mjelde, R., Kasahara, J., Shimamura, H., Kamimura, A., Kanazawa, T., Kodaira, S., Raum, T., Shiobara, H., 2002. Lower crustal seismic velocity-anomalies; magmatic underplating or serpentinized peridotite? Evidence from the Vøring Margin, NE Atlantic. Marine Geophysical Researches 23, 169–183.

Nissen, S.S., Hayes, D.E., Buhl, P., Diebold, J., Yao, B.C., Zeng, W.J., Chen, Y.Q., 1995a. Deep penetration seismic soundings across the northern margin of the South China Sea. Journal of Geophysical Research 100 (B11), 22407–22433.

Nissen, S.S., Hayes, D.E., Yao, B., 1995b. Gravity heat flow, and seismic constraints on the processes of crustal extension: northern margin of the South China Sea. Journal of Geophysical Researcha 100 (B11), 22447–22483.

Pang, X., Yang, S., Zhu, M., Li, J., 2004. Deep-water fan systems and petroleum resources on the northern slope of the South China Sea. Acta Geologica Sinica 78 (3), 626–663.

Qiu, X., Ye, S., Wu, S., Shi, X., Xia, K., Flueh, E.R., 2001. Crustal structure across the Xisha Trough, northwestern South China Sea. Tectonophysics 341, 179–193.

Qiu, X., Shi, X., Yan, P., Wu, S., Zhou, D., Xia, K., 2003. Recent progress of deep seismic experiments and studies of crustal structure in northern South China Sea. Progress in Natural Science 13 (7), 481–488.

Roberts, A.M., Kusznir, N.J., Yielding, G., Styles, P., 1998. 2D flexural backstripping of extensional basins: the need for a sideways glance. Petroleum Geoscience 4, 327–338.

Royden, L., Sclater, J.G., Herzen, R.P.V., 1980. Continental margin subsidence and heat flow: important parameters in formation of petroleum hydrocarbons. American Association of Petroleum Geologists Bulletin 64 (2), 173–187.

Ru, K., Pigott, J.D., 1986. Episodic rifting and subsidence in the South China Sea. AAPG Bulletin 70 (9), 1136–1155.

Sandwell, D.T., Smith, W.H.F., 1997. Marine gravity anomaly from Geosat and ERS 1 satellite altimetry. Journal of Geophysical Research 102 (B5), 10039–10054.

Sclater, J.G., Christie, P.A.F., 1980. Continental stretching: an explanation of the post Mid-Cretaceous subsidence of the central North Sea Basin. Journal of Geophysical Research 85, 3711–3739.

Shi, X., Zhou, D., Qiu, X., Zhang, Y., 2002. Thermal and rheological structures of the Xisha Trough, South China Sea. Tectonophysics 351 (4), 285–300.

Shi, X., Qiu, X., Xia, K., Zhou, D., 2003. Characteristics of the surface heat flow in the South China Sea. Journal of Asian Earth Sciences 22 (3), 265–277.

Steckler, M.S., Watts, A.B., 1978. Subsidence of the Atlantic-type continental margin off New York. Earth and Planetary Science Letters 41, 1–13.

Su, D., White, N., McKenzie, D., 1989. Extension and subsidence of the Pearl River Mouth Basin, northern South China Sea. Basin Research 2, 205–222.

Taylor, B., Hayes, D.E., 1983. Origin and history of the South China Sea Basin. In: Hayes, D.E. (Ed.), The Tectonic and Geologic Evolution of Southeast Asian Seas and Islands 2. American Geophysical Union, Geophysical Monograph, vol. 27, pp. 23–56.

Turcotte, D.L., Schubert, G., 1982. Geodynamics, Application of Continuum Physics to Geological Problems. John Wiley & Sons, New York, p. 432.

Wang, C., 2001. Studies on Oil Generation Conditions, Exploration and Potential Zones of the Southern Regions of the Pearl River Mouth Basin. China Offshore Oil Nanhai East Corporation (Internal Report, in Chinese).

Wang, J., Wu, J., Chen, B., 1997. Synthetical Geophysical Researches of the Basement Structural of the Pearl River Mouth Basin and Donghai Shelf Basins. Tongji University Press, Shanghai, pp. PP35–PP45 (in Chinese).

Watts, A.B., 2001. Isostasy and Flexure of the Lithosphere. Cambridge University Press, Cambridge, pp. 285–338.

Watts, A.B., Stewart, J., 1998. Gravity anomalies and segmentation of the continental margin offshore west Africa. Earth and Planetary Sciences Letters 156, 239–252.

Watts, A.B., Torne, M., 1992. Crustal structure and the mechanical properties of extended continental lithosphere in the Valencia

Trough (western Mediterranean). Journal of Geological Science (London) 149, 813–827.

Weissel, J.K., Karner, G.D., 1989. Flexural uplift of rift flanks due to mechanical unloading of the lithosphere during extension. Journal of Geophysical Research 94, 13919–13950.

Wessel, P., Smith, W.H.F., 1995. New version of the Generic Mapping Tools (GMT) version 3.0 released. Transaction AGU, Eos 76, 329.

White, R.S., McKenzie, D., 1989. Magmatism at rift zones: the generation of volcanic continental margins and floor basalts. Journal of Geophysics Research 94 (B6), 7685–7729.

Whitmarsh, R.B., Manatschal, G., Minshull, T.A., 2001. Evolution of magma-poor continental margins from rifting to seafloor spreading. Nature 413, 150–154.

Xia, K., Zhou, D., 1993. The geophysical characteristics and evolution of northern and southern margins of the South China Sea. Geological Society of Malaysia, Bulletin 33, 223–240.

Yan, P., Zhou, D., Liu, Z., 2001. A crustal structure profile across the northern continental margin of the South China Sea. Tectonophysics 338, 1–21.

Yao, B.C., Zeng, W.J., Hayes, D.E., Spangler, S., et al., 1994. The Geological Memoir of South China Sea Surveyed Jointly by China and USA. China University of Geosciences Press, Wuhan, pp. 34–140 (in Chinese).

Yu, H., 1997. Characteristics of geological provinces in the offshore area around Taiwan. Ti-Chih 17 (1–2), 47–68.

Zhou, D., Ru, K., Chen, H.Z., 1995. Kinematics of Cenozoic extension on the South China Sea continental margin and its implications for the tectonic evolution of the region. Tectonophysics 251, 161–177.

Zou, H., Li, P., Rao, C., 1995. Geochemistry of Cenozoic volcanic rocks in Zhujiangkou Basin and its geodynamic significance. Geochimica V24, 33–45 (Suppl, in Chinese).